FEATURE

Advances in Real-Time Plasma Boundary Reconstruction

From gaps to snakes

By Alessandro Beghi and Angelo Cenedese

The efficient and safe operation of large fusion devices relies on accurate knowledge of the position and shape of the plasma column inside the vacuum chamber. There are several reasons for optimizing plasma shape and position, namely, to maintain adequate clearance from the chamber wall to avoid high densities of power and particle deposition, to be sufficiently close to the wall to ensure adequate passive stabilization, to achieve efficient radio frequency (RF) heating by maximizing antenna coupling (see "Tutorial 9"), and finally, to reduce magnetohydrodynamic (MHD) activity (see "Tutorial 2" in [1]).

Unfortunately, plasma shape is not a directly measurable quantity and thus can only be evaluated using diagnostic data, such as the magnetic measurements of flux and field. Current trends in existing fusion plants, as well as operating scenarios envisioned for future tokamaks, present the control engineer with the challenge of regulating highly unstable, strongly shaped plasmas with precision and reliability. Therefore, whether to improve fusion performance or to protect the machine components, the problem of reconstructing the plasma boundary is critical for both diagnostic and control purposes. In this respect, shape estimation assumes a key role in fulfilling the requirements for real-time applications.

Overview of Methods for Shape Estimation

The Equilibrium Problem

Today, the tokamak is the most common machine for fusion research, used to magnetically confine a gas in the plasma state inside a doughnut-shaped (a torus) metallic

1066-033X/05/$20.00©2005IEEE

chamber. The principle underpinning the design of the tokamak is that it is possible to induce a longitudinal (toroidal) current inside the gas by using the plasma ring as the secondary circuit of a transformer. The consequent creation of a poloidal magnetic field (see "Tutorial 1" in [1]) acts together with an externally imposed toroidal field to produce a magnetic cage that traps the ionized particles. In particular, the magnetic configuration is characterized by the presence of a toroidal field B_ϕ that is nearly an order of magnitude more intense than the poloidal component $B_{\rm pol}$. Consequently, the magnetic lines that guide the particles around the major axis of the torus are helices, which rotate slowly in the toroidal direction. In doing so, the magnetic lines map out nested toroidal surfaces corresponding to constant values of the poloidal magnetic flux $\psi_{\rm pol} = \int \vec{B} \cdot {\rm d}\vec{S}_{\rm pol}$, as well as constant pressure (iso-surfaces). The resultant magnetic field confines a plasma of positive pressure by creating a force equilibrium between the kinetic (gas) pressure and the magnetic pressure (see Figure 1). The poloidal flux, which is given in "Tutorial 1" in [1], is the flux of the magnetic field through a circle concentric with the axis of the torus. The quantity ψ, which is equal to the poloidal flux per radian $\psi = \psi_{\rm pol}/2\pi$, is used to label the iso-surfaces inside the plasma volume.

Assuming an axisymmetric plasma ("Tutorial 3" in [1]) in a cylindrical coordinate system $\{r, \phi, z\}$ (see Figure A in "Tutorial 1" in [1]), the MHD equations obtained by coupling Maxwell's laws with those of fluid mechanics specialize to the partial differential equation

$$\Delta^* \psi = -\mu_0 r J_\phi, \tag{1}$$

where J_ϕ is the toroidal current density (total current $\vec{J} = J_\phi \vec{e}_\phi + J_{\rm pol}\vec{e}_{\rm pol}$, with $\vec{e}_\phi$ and $\vec{e}_{\rm pol}$ unit vectors) and Δ^* is the elliptic operator

$$\Delta^* \psi \equiv \frac{\partial^2 \psi}{\partial z^2} + r \frac{\partial}{\partial r}\left(\frac{1}{r}\frac{\partial \psi}{\partial r}\right).$$

The *equilibrium problem* is to determine from external magnetic measurements the distribution of flux ψ and toroidal current density J_ϕ over the plasma and vacuum region given the configuration of the external coil currents.

By using the momentum equation, which gives the equilibrium between the gradient of the kinetic pressure p and the electromagnetic force $\vec{J} \times \vec{B}$, the Grad-Shafranov equation (see "Tutorial 15" in [2]) derived from (1) has the form

$$\Delta^* \psi = -\mu_0 r^2 \frac{dp}{d\psi} - F\frac{dF}{d\psi}. \tag{2}$$

According to Ampère's law, the auxiliary function $F(\psi) = rB_\phi(\psi)$ is proportional to the poloidal current $I_{\rm pol} = 2\pi F/\mu_0$ flowing in the plasma. Relation (2) describes the equilibrium for an isotropic (showing the same physical properties in all directions) plasma given a particular choice of p and F, which also set boundary conditions at the coordinate frame origin $r = 0$ and at infinity. For a more detailed derivation, see [3] and [4]. This formulation can be extended to various domains, where magnetic flux is present. To begin with, it can be observed that, according to Poisson's equation, the term $\Delta^*\psi$ is equal to zero in the vacuum region. Moreover, $\Delta^*\psi$, which can be expressed as a flux-dependent term in any ferromagnetic materials that may be present, is proportional to the circuit currents $J_{\phi,ext}$ in the poloidal shaping coils or in other conductor domains. To summarize,

$$\Delta^*\psi = \begin{cases} -\mu_0 r^2 p' - FF' & \text{in the plasma domain} \\ -\mu_0 r J_{\phi,\rm ext}(r,z) & \text{in the external conductor domain} \\ \Gamma_\mu(r,z,\psi) & \text{in ferromagnetic materials} \\ 0 & \text{in vacuum,} \end{cases}$$

where the term Γ_μ accounts for the magnetization curve of the material.

The Plasma Boundary

How do we recognize a mass of highly pure and rarefied conductive plasma placed in the vacuum chamber? In other words, how do we define and estimate the *boundary* of the plasma?

A practical definition of the plasma boundary, which comes from the physics of the problem, is associated with the magnetic configuration of the plasma: The boundary is the outermost closed flux surface entirely contained inside the vacuum vessel (Figure 2). Particles interior to

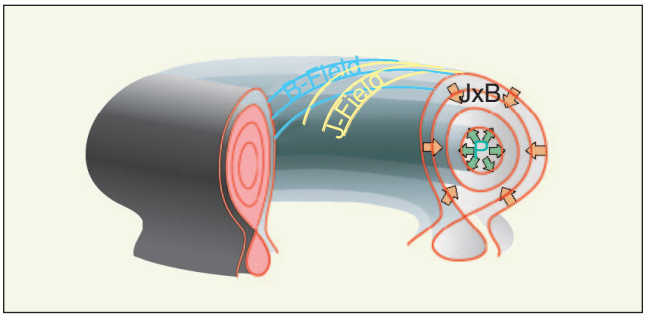

Figure 1. *Plasma surfaces. Nested surfaces, which are loci of constant flux and pressure, are present inside the plasma. The magnetic (B-field) and the current (J-field) lines, which are orthogonal to the pressure gradient ∇p, lie on these surfaces, as do the orbits of the ionized particles. The green arrows represent the kinetic or gas pressure seeking to expand the plasma, while the orange arrows represent the magnetic forces that apply a balancing pressure.*

the plasma boundary follow magnetic field lines [1, Figure 8] that remain in the plasma interior, while field lines external to the boundary intersect with material structures; particles that follow the external field lines eventually collide with these structures. Topologically, the boundary is either the outermost flux contour not intersecting any solid object or it is a *separatrix*, that is, a surface containing an X point (Figure 2), which is a point at which the poloidal magnetic field is zero, or, equivalently, the flux function presents a saddle point. The X point often exists independently of whether it is a part of the most external closed flux surface.

For an axisymmetric plasma there is no loss in validity in limiting the analysis to a poloidal cross section of the machine. Two domains of interest can be identified on the poloidal plane Ω, as shown in Figure 2:

- Ω_I is the region enclosed by the shaping coil locations
- the subset Ω_P of Ω_I is the *plasma region*, defined as the vacuum region interior to the containment vessel, where plasma may exist.

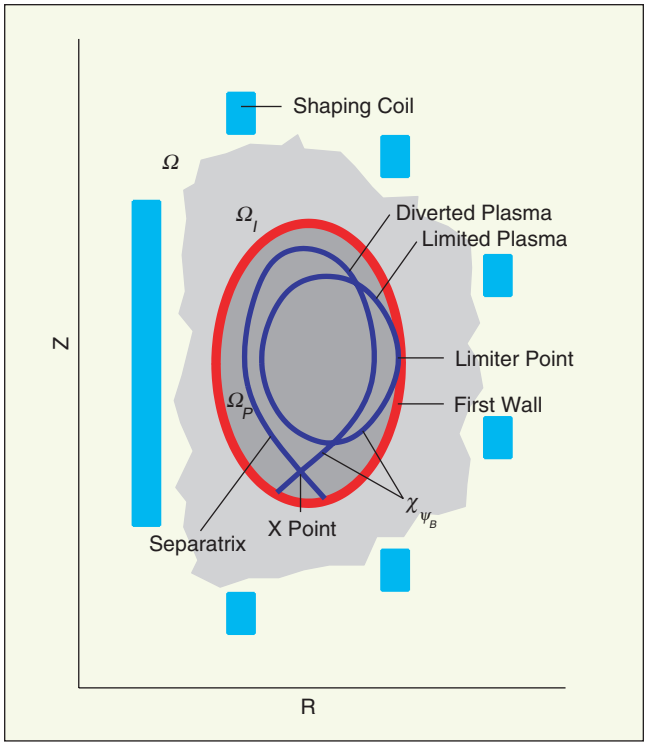

Figure 2. *Poloidal cross section of a tokamak machine. In the poloidal plane Ω, the domain Ω_I is the region within the shaping coils, while the plasma region is Ω_P. The plasma boundary is defined as the most external closed flux surface entirely contained in the vessel. The magnetic configuration can be either a diverted or a limited plasma. In a diverted plasma, the plasma boundary flux is determined by the magnetic null location, where the boundary forms an X point. In a limited plasma, the plasma touches the first wall at the limiter point, which determines the boundary flux. The flux value is ψ_B at the boundary surface χ_{ψ_B}.*

The flux function ψ defined in the domain Ω_I is a real-valued function of r and z monotonically decreasing from the center of the plasma toward the edge. The boundary flux value ψ_B, which identifies the plasma boundary surface χ_{ψ_B}, is determined by comparing the flux value ψ_X at the X point with the maximum value $\psi_{\text{firstwall}}$ of the flux along the first wall, which is constituted by the plasma facing structures. When the X-point flux is higher than $\psi_{\text{firstwall}}$, the separatrix is internal to every flux surface touching the wall, and, consequently, the plasma boundary coincides with the part of the separatrix inside the plasma domain Ω_P (Figure 2). In this case, the plasma is in a *diverted configuration*. Otherwise, the plasma is a *limited plasma*, physically touching the first wall at the limiter point P_{limiter} characterized by $\psi\,(P_{\text{limiter}}) = \psi_{\text{firstwall}}$ (see "Tutorial 7").

The *boundary reconstruction problem* is to locate the plasma inside the vacuum vessel and determine the plasma boundary position with respect to the first-wall components. Clearly, the equilibrium problem and the boundary reconstruction problem are intimately connected. It is important to stress that the plasma is seen and investigated only through the eyes of a privileged magnetic descriptor, namely the flux function, which contains all of the information needed for reconstructing the boundary position. At the same time, complete knowledge of the external field configuration facilitates the reconstruction of the plasma location but not the reconstruction of interior details.

Reconstruction and Shape Description for Shape Control

Once the equilibrium problem and the boundary definition have been formulated, the focus of attention is on understanding how the plasma and boundary shape evolve in time, as well as the possible magnetic configurations. A complete answer to these questions lies in the solution of a *free boundary problem*, since the differential equation governing the equilibrium (2) is defined in a domain whose boundary is not given a priori and is part of the unknown. The free boundary problem is often solved using finite difference or finite element techniques, whose implementation sometimes involves adaptive meshing procedures to follow the plasma deformation. Nonlinear equilibrium evolution codes, such as PROTEUS [5] and MAXFEA [6], reconstruct the shape and simulate the plasma dynamics for a plasma discharge. Nonetheless, in these electromagnetic codes, the exacting task of modeling the physical phenomena often requires iterative procedures that are computationally intensive. Indeed, considering these aspects and the inherent features of finite element methods, while the equilibrium evolution codes represent a valuable tool for simulating plasma behavior and designing and validating controllers, real-time use is not practical.

Consequently, we describe an alternative approach to reconstructing the boundary shape during the pulse, using procedures that fit simplified analytical models to magnetic

measurements. More generally, semianalytical procedures can be developed to approximate the plasma flux distribution with a suitable number of current filaments [7] or finite elements [8] placed inside the vacuum vessel. Related algorithms use multipolar expansions to describe the magnetic configuration [9] (a multipolar expansion can be thought of as a Taylor expansion of the function ψ). In this regard, it is important to distinguish among *equilibrium evolution codes* such as MAXFEA and PROTEUS, *equilibrium reconstruction codes* (EFIT [10]), and *boundary reconstruction codes* (XLOC [11]). The equilibrium evolution codes *evolve* the equilibrium, based on the dynamics of the external coil currents and either a bulk or distributed plasma current, while equilibrium reconstruction codes *solve* the equilibrium problem, taking into consideration internal measurements and the actual plasma current distribution. Both types of codes provide a complete magnetic description of the plasma, which includes both the plasma current density distribution and the flux distribution. A primary difference between the two classes of codes concerns the input data, since equilibrium reconstruction codes use experimental measurements and the resulting accuracy is limited because of ill-posedness of the problem and measurement noise. On the other hand, the data for the equilibrium evolution codes are provided by the code itself, in the form of simulated currents in all conductors, including plasma, and is therefore perfectly known, at least in principle. Finally, boundary reconstruction codes are limited to locating the boundary and do not aim at a detailed analysis of the internal plasma features.

Tutorial 6: Divertors

The helium byproduct of the fusion reaction (sometimes called *helium ash*) must be removed from the vacuum chamber to prevent the by-product from interfering with subsequent fusion reactions. The method selected for accomplishing the removal is to use one or more divertor regions (divertors) with pumping. The figure below shows the divertor in the JET tokamak. The idea of the divertor is to divert nonhydrogen particles away from the plasma to a region that is designed to safely absorb their heat and remove them from the plasma chamber. All particles, including the helium ash, tend to remain in the plasma for only a finite time known as the *confinement time* (see "Tutorial 2" in [1]) before leaking out. When the helium nuclei leave the plasma, they are still charged and therefore tend to follow magnetic field lines. Other impurities, as introduced by the plasma interacting with device components, are also ionized and follow the field lines. The region just outside the separatrix (last closed flux surface) where this occurs is known as the *scrape-off layer* (SOL). Field lines outside of the separatrix do not close inside the vacuum vessel. Instead, they terminate on the interior plasma-facing wall of the vacuum vessel (the *first wall*) at locations known as the *strike points* (see the figure above). As a consequence, the impurity and helium ions follow these first few external field lines until they contact the wall in the divertor region, and they are then pumped out of the tokamak chamber. The particles contacting the plasma facing materials at the strike points are still very high energy, so divertors are specifically designed to withstand this continuous bombardment of high energy particles. Divertors are always constructed of heat-resistant materials and often incorporate geometric designs intended to widen the area that is impacted by the particles.

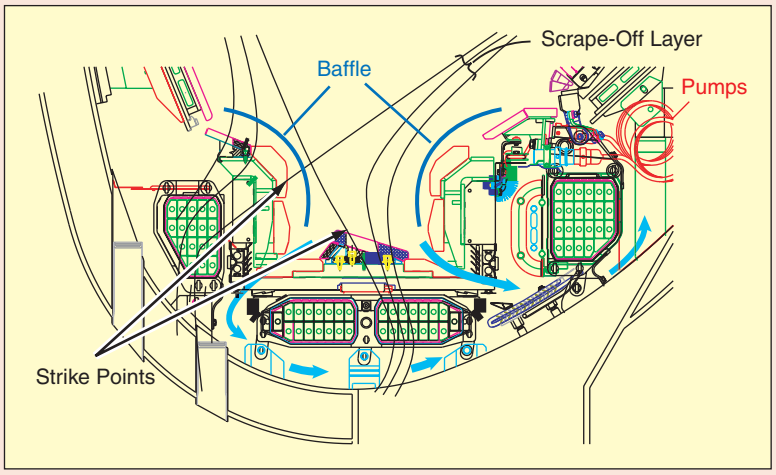

The divertor region in the JET tokamak. A set of flux contours is shown to represent the plasma. The divertor baffles serve to direct particles flowing in the scrape-off layer into the throat of the divertor, where they can be pumped out (light blue arrows). Cross sections of the four divertor coils for JET can be seen just outside the divertor. Each small green rectangle inside a coil represents a single turn of the multiturn winding used to multiply the flux produced by the coil. The small circles inside these rectangles are the channels used for water cooling. (Courtesy of EFDA/JET.)

The Fitting Codes EFIT and XLOC

The EFIT code [10] is an equilibrium reconstruction algorithm that fits the equilibrium model (2) to the external magnetic measurements and to internal diagnostic data. The solution, which satisfies the Grad-Shafranov model, accounts for a distributed current source in the plasma

Tutorial 7: Limiter and Divertor Configurations

When the first tokamak experiments were conducted in the former Soviet Union, it was observed that the vacuum vessel was not sufficient to maintain a pure plasma. Some improvement could be obtained by limiting the plasma with the insertion of a material structure (called a *limiter*) just inside the chamber (see Figure A). In this way, the external layer of the plasma magnetic lines are intercepted by the limiter, and the last closed flux surface is kept separated from the first wall. In other words, the mechanical limiter protects the chamber from plasma bombardment and serves to define the edge of the plasma. Nevertheless, the fluxes of particles that collide with the limiter structure are highly energetic and thus can dislodge atoms from the surface material through a process called *sputtering*. Therefore, when designing a limiter, it is important to choose an appropriate material, such as tungsten, molybdenum, or graphite, to ensure power load management and durability, and to design for easy replacement. At the same time, efficient pumping is needed to remove the impurities created by the sputtering and prevent plasma pollution (cryocondensation pumps are usually employed to this aim).

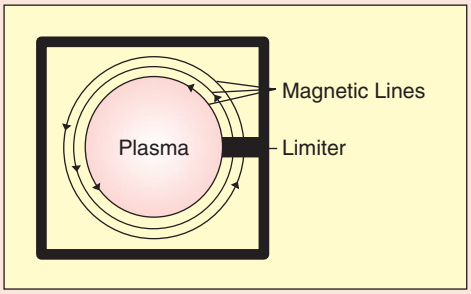

Figure A. *The limited plasma configuration. This configuration is generated by inserting, in the vessel, the limiter, a mechanical object that intercepts a fraction of magnetic lines and creates a separation between the main plasma and the facing structures. In doing so, plasma pollution due to impurities from the first-wall is reduced, and the last closed flux surface bounding the plasma volume is defined.*

These issues led to the development of an interface between the plasma and the facing components, without using a mechanical limiter. The magnetic divertor (see "Tutorial 6") is a structure that creates a magnetic configuration where the external layer of magnetic lines is guided away from the main plasma and collides onto a collector plate. A poloidal divertor is obtained by placing several coils near the plasma surface, with a current parallel to that of the plasma and flowing in the opposite direction (*flux expansion coils* in Figure B), to generate a local field that opposes the poloidal field in the plasma. Consequently, the resulting magnetic field is locally characterized by the presence of a null point (X point), and thus a magnetic separatrix is created (see Figure B). Since, in most tokamaks, the pulse duration is much longer than the particle containment time, during the discharge, on average, each plasma ion drifts toward the wall and returns to the plasma many times (plasma recycling). Using the divertor configuration, the recycling properties of the plasma are generally improved because the collector plates are more remote than in the limiter case. For this same reason, by controlling the flux expansion coil currents (Figure B), the magnetic lines can be spread over a wider area on the material structure, thus leading to a lower maximum power density impinging on the structure and longer times between replacement of the plates.

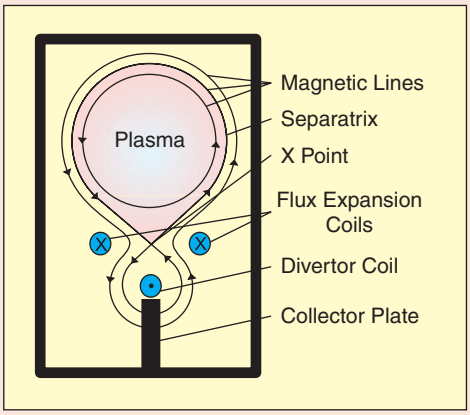

Figure B. *The diverted plasma configuration. The divertor locally modifies the magnetic lines so that the main plasma does not contact the vessel. With this configuration, a magnetic null called the X point is present; the magnetic surface defining the plasma boundary is referred to as the separatrix. The magnetic lines external to the plasma boundary collide onto a collector plate equipped with cryocondensation pumps to remove impurities, which could reenter the plasma.*

Furthermore, it has been shown, by the theory of plasma physics, that the shape of the plasma is of great importance in determining fusion performance and that the interaction with the first wall plays a fundamental role. In particular, it has been observed that the formation of a magnetic separatrix inside the vacuum vessel facilitates the transition toward a high-confinement regime (the H-mode), while increasing the plasma temperature and the energy confinement time (see "Tutorial 2" in [1]), for the same input power.

region and is given by the pair (ψ, J_ϕ), where the distribution ψ of flux on the poloidal plane along with the toroidal plasma current J_ϕ provide the least-squares fit to the data consistent with (2).

Each magnetic measurement in EFIT (see "Tutorial 8") is defined as the sum of two contributions, due to the external coil currents I_{ext} and the plasma current J_ϕ. A measurement C at a generic point P_j in the domain Ω_I is obtained from the current sources placed at locations $\{P_i\}$ by means of Green's functions G, where $C_{P_j} = G(P_j, P_i)\, I_{P_i}$ [12]. The solution to the reconstruction problem is obtained from an iterative algorithm that estimates at iteration $m+1$ the magnetic measurement $C^{(m+1)}$ (for more details, see "Tutorial 8"), using the flux $\psi^{(m)}$ in the plasma domain $\Omega_P^{(m)}$ calculated in the previous step m. Hence, an iteration step in the EFIT algorithm is given by

$$C_{P_j}^{(m+1)} = \sum_{i=1}^{N_{\text{ext}}} G(P_j, P_i)\, I_{\text{ext}} + \iint_{\Omega_P^{(m)}} G(P_j, P)\, J_\phi\left(P, \psi^{(m)}\right) \mathrm{d}P.$$

The signals obtained from EFIT are then compared with data from magnetic sensors, and, to obtain the axisymmetric plasma current, the reconstruction algorithm minimizes the quadratic error

$$\chi^2 = \sum_{k=1}^{N_{\text{meas}}} \left(\frac{M_k - C_k}{\sigma_k}\right)^2 \tag{3}$$

on the diagnostic data weighted with the variance σ_k of the measurement, where M_k and C_k are the magnetic sensor measurement and the reconstructed signal, respectively. The optimization procedure is then interleaved with the solution of the equilibrium problem

$$\Delta^* \psi^{(m+1)} = -\mu_0 r J_\phi\left(\psi^{(m)}\right) \tag{4}$$

to update the flux function. This procedure is less computationally expensive than trying to directly solve the nonlinear problem defined by (2) but not sufficiently fast for real-time use. Adjustments are thus made to the algorithm so that a one-iteration scheme can follow the plasma evolution during the pulse.

The modified real-time EFIT shape identification method is implemented as a two-loop routine [13], where a fast loop performs the least-squares fit (3) and generates the error signals as inputs to the controller, comprising the flux values at a predefined set of control points. A more complex portion of the algorithm is required to solve the equilibrium problem (4). Consequently, the flux errors fed to the control algorithm are provided through a fit procedure that uses newly acquired diagnostic data in (3) and a flux data set from (4) based on previously obtained measurements. Thus, the error-signal inputs for the real-time control system partly inherit this older information.

A fitting scheme based on local expansions has been developed at JET and incorporated in the XLOC code, which is devoted to real-time boundary reconstruction [11]. In XLOC, the magnetic flux function is extrapolated into the vacuum region (external to the plasma boundary) by fitting the available sensor measurements to the vacuum equation $\Delta^* \psi = 0$, thus overcoming the unwieldy task of plasma modeling. The information is then postprocessed by a second module that reconstructs the plasma shape in terms of boundary to first-wall distances called *gaps*.

The XLOC code represents the magnetic flux ψ on the poloidal plane with several polynomial functions of high degree, each locally defined over connected domains surrounding the plasma (Figure 3). This procedure imposes continuity constraints that provide smooth transitions. Having defined basis functions in terms of powers of the plane coordinates (r, z), that is $\{1, r, r^2, \ldots, rz, r^2 z, \ldots\}$, and by constraining the local flux equations to satisfy the vacuum condition $\Delta^* \psi = 0$, the polynomial model $\widehat{\psi}$ can be written in matrix form as

$$\widehat{\psi}(r, z) = f(r, z)^T A, \tag{5}$$

where the components of the vector $A = [a_{0,0}, a_{1,0}, a_{2,0}, \ldots, a_{1,1}, a_{2,1}, \ldots]^T$ are polynomial coefficients and $f(r, z) = [1, r, r^2, \ldots, rz, r^2 z, \ldots]^T$. A linear problem with unknowns $\{a_{i,j}\}$, which can be determined from measurements of the flux ψ, is defined in (5). The coefficients $\{a_{i,j}\}$ are calculated by fitting the polynomial model function to a vector M of sensor measurements with known (r, z) coordinates. Since the magnetic configuration in the X-point region is strongly influenced by the current flowing in the divertor coils, this information is explicitly inserted in the model. The flux contribution ψ_{div} at location P_j due to the divertor coil currents can be computed by means of precalculated Green's functions G

$$\psi_{\text{div}}(P_j) = \sum_{i=1}^{N_{\text{div}}} G(P_j, P_i)\, I_{\text{div}}(P_i),$$

where the N_{div} divertor sources are placed at P_i. Excluding ψ_{div} from the fitting procedure improves the convergence and increases the precision of the fit, that is,

$$\widehat{\psi}(r, z) = \psi_{\text{div}}(r, z) + f(r, z)^T A. \tag{6}$$

The vector M of measurements from sensors of various types, such as flux loops, pickup coils, and saddle loops

(see "Tutorial 8"), can be reconstructed from the flux function (6) and expressed using polynomial functions $g_{\text{flux}}(r,z)$, $g_{\text{pickup}}(r,z)$, and $g_{\text{saddle}}(r,z)$ deduced from $f(r,z)$. The sensor measurements s_{flux}, s_{saddle}, and s_{pickup} [(1)–(3) in "Tutorial 8"] can be expressed as

$$s_{\text{flux}}(P) = \psi_{\text{div}}(P) + \underbrace{f(P)^T A}_{g_{\text{flux}}(P)^T A},$$

$$s_{\text{saddle}}(P_1, P_2) = [\psi_{\text{div}}(P_1) - \psi_{\text{div}}(P_2)] + \underbrace{\left[f(P_1)^T A - f(P_2)^T A\right]}_{g_{\text{saddle}}(P_1,P_2)^T A},$$

$$s_{\text{pickup}}(P,\theta) = \underbrace{-\frac{1}{r}\left[\frac{\partial\left(\psi_{\text{div}}(P) + f(P)^T A\right)}{\partial z}\sin\theta\right]}_{g_{\text{pickup}}(P,\theta)^T A} + \underbrace{\frac{\partial\left(\psi_{\text{div}}(P) + f(P)^T A\right)}{\partial r}\cos\theta\Bigg]}_{g_{\text{pickup}}(P,\theta)^T A},$$

where $P = (r,z)$, $P_1 = (r_1, z_1)$, and $P_2 = (r_2, z_2)$ indicate the sensor positions, and θ is the orientation of the pickup coils. By grouping g_{flux}, g_{saddle}, and g_{pickup} into a vector g_M and placing the ψ_{div} calculated contributions into a vector $\psi_{M,\text{div}}$, the least-squares fit using the sensor measurement vector M is obtained from

$$\min_A \left\| \psi_{M,\text{div}} + g_M^T A - M \right\|_2,$$

which yields the polynomial coefficients $\{a_{i,j}\}$ for the model $\widehat{\psi}$ of the flux map [Figure 3(b)].

Next, the X point is located by searching for the zero of the magnetic field in a predetermined box superimposed on the divertor region [Figure 3(a)]. The limited-diverted plasma distinguishing procedure (see the discussion in "The Plasma Boundary" section) is then carried out by comparing the flux value at the X point with the values at predefined first-wall locations to obtain the flux at the boundary ψ_B. A set of gap lines is chosen by selecting a group of segments that start at the first wall and end near the center of the vacuum chamber as

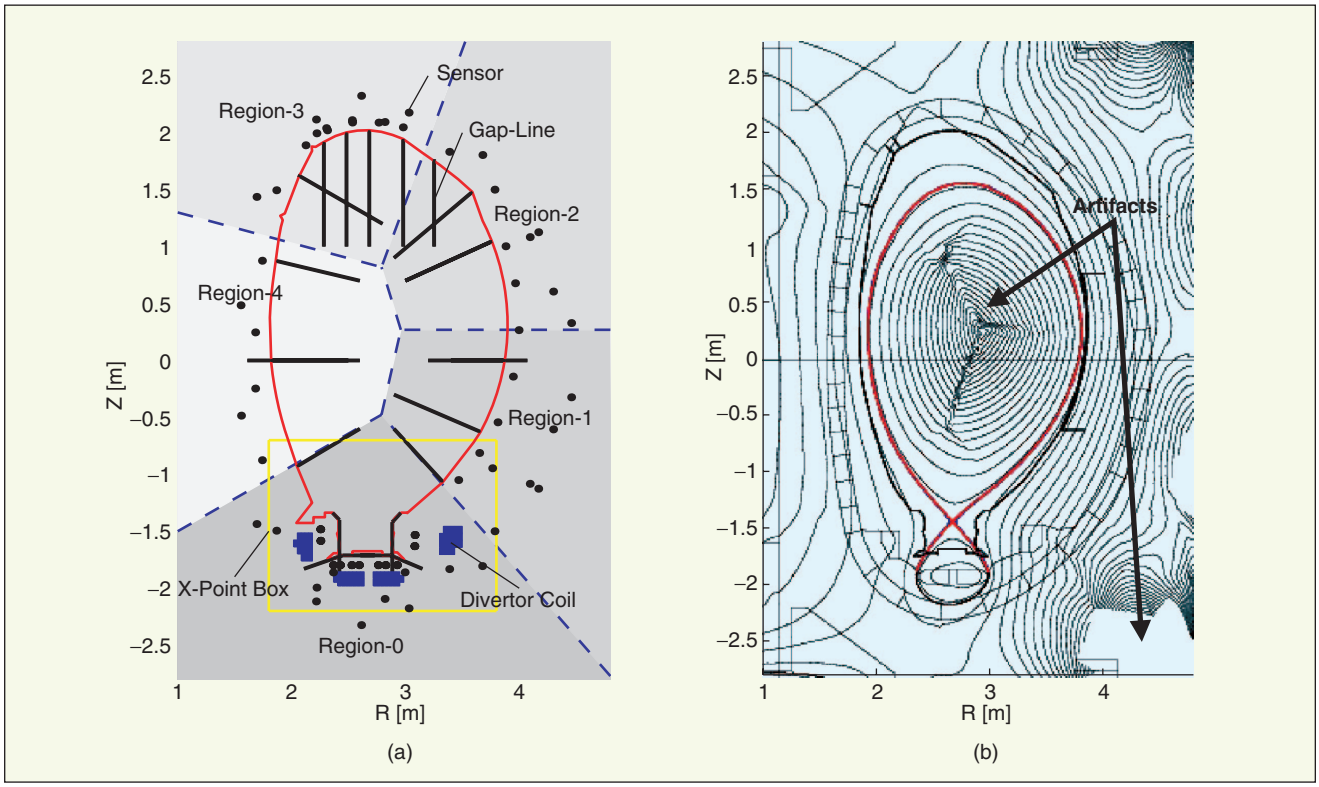

Figure 3. *JET cross sections that illustrate operation of the XLOC code. (a) The partition of the poloidal plane and the gap locations. The gap lines and the magnetic sensors are indicated with solid lines and dots, respectively. The gap values at JET are computed as the distances between the interior wall of the containment vessel (shown) and the plasma boundary along the illustrated gap lines. The divertor coil sections are visible in the lower part of the machine, and the box for the X-point search is highlighted. (b) The output flux map of the XLOC code postprocessed with a contour routine. Artifacts due to the polynomial approximation and the lack of a plasma model are evident.*

Tutorial 8: Magnetic Diagnostics

In a fusion device, magnetic measurements are usually separated into two different classes, namely, field and flux measurements, both of which are obtained by using sensors placed outside the plasma boundary but within the external magnetic field created by the plasma.

Typical magnetic sensors produce a voltage V_0 that is proportional to the time derivative dm/dt of a physical quantity m. For example, m might be a current in amps or a flux in webers. The voltage $V_0 = k(dm/dt)$ is integrated by a hardware integrator circuit to obtain $V_1 = \int V_0\, dt = km$. The integration is usually followed by one or more processes (amplifiers, voltage dividers, digitizers), whose net effect is to multiply V_0 by a gain G to obtain $V_2 = GV_1 = Gkm$. Multiplication by $1/(Gk)$ converts from the integrated volt-second signal to physical units. The multiplier k depends on the type of device. Examples of tokamak magnetic sensors are shown in the figure (right).

The magnetic flux ψ_{pol} is measured by integrating the electromotive force induced in a full flux loop placed outside the vacuum vessel in the toroidal direction. Flux loops consist of a single loop of wire connected to a voltage sensor. The integrated voltage represents the total (poloidal) flux ψ_{pol} through the loop. For an axisymmetric plasma, this measurement provides the value of the flux in a specific position of the poloidal plane. For flux loops, $k = 1$ can be used to represent flux directly in volt-seconds or webers. Some devices use $k = 2\pi$ to convert from total flux ψ_{pol} in weber to flux ψ in webers per unit radian.

Saddle loops also measure total magnetic flux, and, by assuming nearly constant flux across the loop, a measurement of the magnetic field normal to the loop surface is obtained. A saddle loop can be constructed by connecting two sectors of flux loops. At JET, the use of saddle loops on the surface of the vessel provides, for a perfectly axisymmetric plasma, measurements of flux differences between two locations on the poloidal plane.

The magnetic B-field measurement is performed using inductive sensors (known as *magnetic probes*, *B-probes*, *magnetic pick-up coils*, or just *pick-up coils*) that measure the flux variation induced in a coil, so that the flux variation is proportional to the field at the sensor location. Magnetic probes consist of multiple windings of wire in a small (a few centimeters) radius, connected to a voltage sensor. The integrated voltage represents local (poloidal) magnetic field using the relationship $\psi = \int B\, dA/2\pi$, where ψ is the flux per unit radian. This expression is an approximation since the flux is not perfectly constant across the open end of the probe. For magnetic probes, the proportionality constant k is given by $k = NA$,

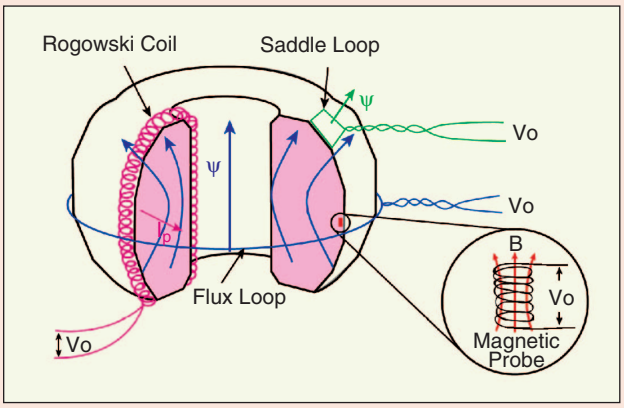

Magnetic diagnostics. All of these sensors operate on the same basic principle, namely, changing flux induces a voltage in a coil of wire. This voltage is integrated to determine the flux through the coil.

where N is the number of turns and A is the cross-sectional area (see the figure above).

Taking the JET tokamak as an example, each measured signal s is related to the flux ψ by the equations

$$s_{\text{flux}}(r, z) = \psi(r, z), \tag{1}$$

$$s_{\text{saddle}}(r_1, z_1, r_2, z_2) = \psi(r_1, z_1) - \psi(r_2, z_2), \tag{2}$$

$$s_{\text{pickup}}(r, z, \theta) = -\frac{1}{r}\left[\frac{\partial \psi(r, z)}{\partial z}\sin\theta + \frac{\partial \psi(r, z)}{\partial r}\cos\theta\right], \tag{3}$$

where, considering the poloidal cross section of the machine (ϕ = constant), (r, z) is the sensor location for the flux loops and pickups, (r_1, z_1) and (r_2, z_2) are the locations of the toroidal limbs of the saddles, and θ is the orientation of the pickup coils; (3) is based on the flux-field relation given by

$$B_r(r, z) = -\frac{1}{r}\frac{\partial \psi(r, z)}{\partial z},$$

$$B_z(r, z) = \frac{1}{r}\frac{\partial \psi(r, z)}{\partial r}.$$

Finally, as shown in the figure, Rogowski coils measure toroidal plasma current (I_p) plus currents in the vessel by computing a line integral of magnetic field in a closed loop around the current path. For Rogowski loops, the proportionality constant k is given by $k = N\mu_0 nA$, where n is the number of turns per unit length, A is the cross-sectional area of a single coil turn, and N is the total number of coil turns around the current path being measured.

shown in Figure 3(a). The flux function is computed along each gap line, and a point is determined whose flux value corresponds to the boundary flux value. The distance from this point to the beginning of the gap line is defined as the *gap value*. The XLOC code constructs a discretized representation of the plasma boundary through this sequence of points (gaps) and passes this information to the shape controller. The effect of neglecting the plasma current in the modeling is visible in Figure 3(b). In particular, the validity of the flux map reconstruction is local and limited to the exterior of the plasma, while artifacts are formed in the interior of the plasma.

Employed in DIII-D and JET, the real-time EFIT and XLOC codes have proven to be efficient for producing real-time shape information. Moreover, these algorithms use different representations to describe the plasma boundary and interface with the controller, namely, flux values (real-time EFIT) or gaps (XLOC).

The Shape Descriptors

At this stage, we make a distinction between *shape estimation* and *shape reconstruction*. *Shape reconstruction* refers to a full description of the plasma shape, including the continuous boundary curve, which can be obtained by using nonlinear equilibrium codes, while *shape estimation* provides only a discrete description of the shape for control purposes. The representation of the boundary measures the *distance in shape* between the actual plasma boundary and the specified target boundary, namely, a metric.

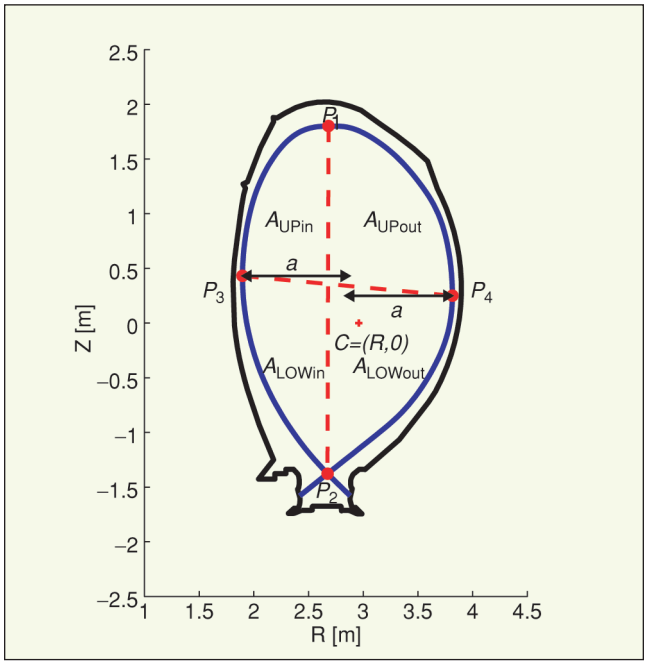

Figure 4. *Operational definitions of the plasma shape global parameters. The main properties of the cross section are shown, including the extreme boundary points (P_1, P_2, P_3, P_4), the center C of the tokamak cross section, and major and minor radii R and a. The area partition (A_{LOWin}, A_{LOWout}, A_{UPin}, A_{UPout}) of the plasma cross section is also shown. Given these definitions, the elongation is operationally obtained as* $\kappa = [z(P_1) - z(P_2)]/[r(P_4) - r(P_3)] = (z_{\max} - z_{\min})/(r_{\max} - r_{\min})$. *Upper and lower triangularity (δ_{UP} and δ_{LOW}) are computed as* $\delta_{\mathrm{UP}} = [r_{\mathrm{av}} - r(P_1)]/a$ *and* $\delta_{\mathrm{LOW}} = [r_{\mathrm{av}} - r(P_2)]/a$, *where* r_{av} *is the average radius between* $r_{\max}$ *and* $r_{\min}$.

Calculation of high-order current moments [14] provides a complete description of the plasma geometry. Given the toroidal current distribution J_ϕ, the position of the current centroid (center of plasma current "mass"), triangularity, and other parameters can be computed through integral calculations as current distribution moments. However, even though the total plasma current is controlled, the distribution of J_ϕ across the plasma depends on less measurable—and less controllable—aspects of the plasma. The difficulty of measuring the internal current distribution and performing integral calculations calls for an alternative computational methodology in which a plasma current model is not used and only the geometry of the shape is taken into account.

The plasma shape is characterized by local properties such as the existence of a poloidal limiter, the distance between the boundary and the first wall, the presence and location of X points, and by global parameters that consider the shape as a whole (see "Tutorial 7"). The concept of gaps as the distance between the plasma boundary and the machine first wall represents an evolution of the basic flux description. The necessity of defining and producing quantities such as gaps, which cannot be directly measured but only calculated, stems from the idea of translating a difference in flux into a spatial distance.

The collection of global shape parameters includes the definition of area of the plasma cross section A, important for estimating the nuclear reaction volume, and other quantities such as the elongation κ and the triangularity δ (defined below), which describe how this area is distributed with respect to the poloidal section. From the physicist's point of view, these features are interesting for developing reactor-relevant scenarios needed to reach high fusion performances. For the control engineer, to define elongation κ and triangularity δ, it is necessary to find suitable mathematical definitions consistent with intuition. Elongation κ is a characteristic of the plasma poloidal cross section [4], defined as the ratio of the plasma sectional area A to the area of a circle having the same minor radius a as the plasma, that is,

$$\kappa = \frac{A}{\pi a^2}, \tag{7}$$

where the minor radius a of a noncircular plasma is defined as the semidistance between the outermost and innermost points of the boundary curve (with reference to

Figure 4, respectively, points P_4 and P_3). The triangularity δ measures the extent to which the plasma is shaped like a triangle. The calculation of these quantities usually depends on local point-based information of the plasma cross section, shown in Figure 4, with points $\{P_1, P_2, P_3, P_4\}$. The elongation is computed as

$$\kappa = \frac{z(P_1) - z(P_2)}{r(P_4) - r(P_3)} = \frac{z_{\max} - z_{\min}}{r_{\max} - r_{\min}}. \tag{8}$$

A similar observation holds also for the upper and lower triangularity parameters

$$\delta_{\mathrm{UP}} = \frac{r_{\mathrm{av}} - r(P_1)}{a}, \tag{9}$$

$$\delta_{\mathrm{LOW}} = \frac{r_{\mathrm{av}} - r(P_2)}{a}, \tag{10}$$

where $r_{\mathrm{av}} \equiv (r_{\max} + r_{\min})/2$ is the average radius.

The cross-sectional area, elongation, and triangularity are approximated in real time during the plasma discharge using information available to the control system. For example, when the boundary is specified by a set of gaps, the position of the boundary curve uppermost point P_1 is approximated from measurements along the gap line that best represent (on average) the plasma top point location. The choice of this gap line is made by analyzing the operating space of plasma configurations attainable in the specific device.

Flux and Gap Descriptions for Shape Control

Given the definition of the plasma boundary, a natural way to control the plasma shape is the *isoflux technique* [15], which consists of regulating the magnetic flux at a set of locations in the poloidal plane using the external coil current sources. The magnetic description provides direct information on the boundary location, and the accuracy of the evaluation of the flux function is reflected in the precision of the shape reconstruction. The plasma shape error is determined by computing the flux error e_ψ relative to a reference value ψ_{ref} at a set of control points on the poloidal plane. The flux error e_ψ at a point P_j, which serves as a control input, can be directly linked to the currents flowing in the plasma I_{plasma}, in the active coils I_{coils}, and in the passive structures I_{vessel} according to

$$\begin{aligned} e_\psi(P_j) = {} & G_{\mathrm{plasma}}(P_j, P_{\mathrm{plasma}})\, I_{\mathrm{plasma}} \\ & + G_{\mathrm{coils}}(P_j, P_{\mathrm{coils}})\, I_{\mathrm{coils}} + G_{\mathrm{vessel}}(P_j, P_{\mathrm{vessel}})\, I_{\mathrm{vessel}}, \end{aligned}$$

where G_{plasma}, G_{coils}, and G_{vessel} are Green's functions. By choosing the control point locations before the pulse sequence begins, a control system based on this approach can drive the plasma current circuit and the shaping coils, and thereby obtain the desired configuration.

The isoflux technique is currently implemented in the DIII-D tokamak [13] by means of a proportional-integral differential (PID) controller whose gain matrices $\{K_P, K_I, K_D\}$ evolve in time to match the designed plasma shape and parameters (see Figure 5). The external voltages V_{ext} are given by

$$V_{\mathrm{ext}} = K_P \begin{bmatrix} e_\psi \\ e_X \end{bmatrix} + K_I \int \begin{bmatrix} e_\psi \\ e_X \end{bmatrix} + K_D \frac{d}{dt} \begin{bmatrix} e_\psi \\ e_X \end{bmatrix},$$

where e_X is the error in the X-point position. Experience has shown that the real-time reconstruction algorithm yields good accuracy compared with the offline full equilibrium reconstruction, and, by accurately placing the flux control points, the system provides sufficient flexibility to explore a wide range of different shapes and configurations.

The gap approach was used at JET to develop a robust multi-input, multi-output feedback control system (see [16]

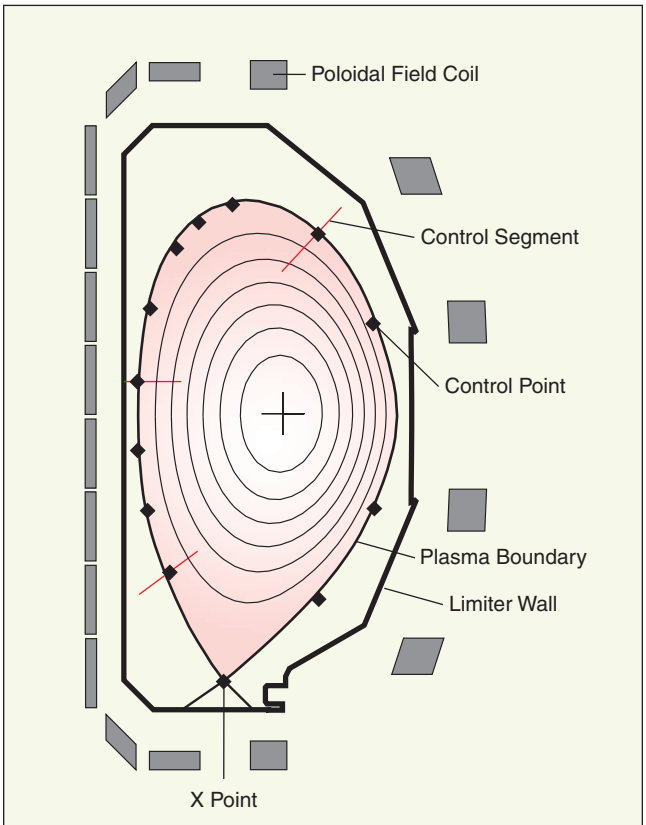

Figure 5. *Layout of the DIII-D tokamak. The poloidal cross section of this tokamak highlights the position of the shaping field coils and the points for the isoflux control system (diamonds). The drawing represents a single null divertor discharge.*

and [17]). Several gap lines were chosen on a geometric basis in accordance with operational needs. The gap calculation module linked to XLOC searches along the gap lines for the boundary flux value to produce a set of plasma to first-wall distances. A schematic picture of JET gap lines, together with the location on the poloidal cross section of the machine is presented in Figure 6(a).

In the framework of the ITER project [Figure 6(b)] [18], several controllers were designed, based on a gap control strategy (see, for example, [19]). In terms of robustness and accuracy, the simulation results demonstrate that a gap controller is an effective approach for controlling the plasma shape in the new machine and for comparing different solutions. These analyses are being used to assess performance of the system to obtain the expected plasma configurations.

Representation of the boundary by a set of distances from the wall introduces new considerations when addressing the design of a shape control system. First of all, while the map between the currents and the flux values can be regarded as linear by neglecting transient effects and nonlinearities in the materials, a linear relation is no longer valid when we consider the gap distances, or X-point location. The most obvious nonlinearity is the transition between the limited and diverted plasma shapes.

Despite the success of the gap control technique in JET and the studies carried out for the ITER design, the local nature of the information inherent in the gap description can lead to ambiguities in the boundary representation. Some details may remain hidden when it comes to determining particular properties of the plasma shape, such as the extreme points of the boundary and the global quantities A, κ, and δ, although the locality of the information is partly overcome by the good behavior and regularity of the boundary shape. Moreover, choosing a discrete number of points to describe and control a continuous curve introduces arbitrariness in the selection of the gap lines. This issue can be minimized, but not completely avoided, by an intelligent and careful procedure for choosing the controlled variables [20], [21]. A further problem arises from the fact that the gap lines are not always normal to the vessel, and thus the gap measurements do not represent the minimum distance from the first wall but rather the distance along a line. In some cases, increasing the gap can cause the plasma to move toward the vessel. Experience and a careful evaluation are fundamental in understanding the gap information and in discerning potentially dangerous situations, but again the intervention of some high-level interpretation is needed.

While adequate for the accuracy requirements in normal plasma operation, the gap description and gap-based control appear to have limited effectiveness in more advanced scenarios, where the control of global quantities such as elongation and triangularity are demanded. In fact, these shape parameters are usually defined in real time using functions of gap values (Figure 4) in place of the original definitions

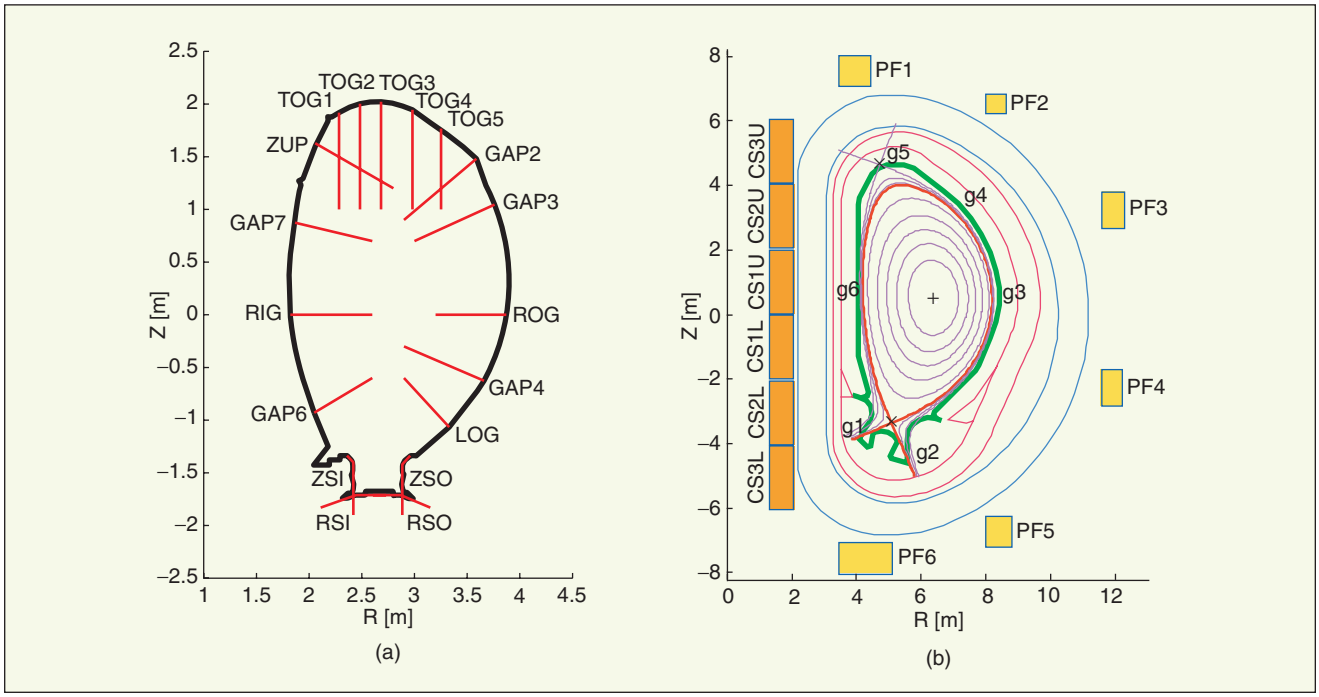

Figure 6. *Gap location for (a) JET and (b) ITER. The gap location is chosen semiempirically at JET according to experimental needs, while for ITER an optimal placement procedure is adopted. In any case, the gap approach suffers from the local nature and arbitrariness in the definition of the gaps.*

(8)–(10). Regulating these gaps may fail to control the behavior of the plasma parameters since local deformations can distort the boundary while preserving the gap values.

A step toward more complete control of the shape has been made at JET by the eXtreme Shape Controller (XSC) project [22]. The XSC, which uses a specific choice of actuators for a particular target plasma, achieves the desired geometry by minimizing the deviation of a dense set of gaps from the target shape (see also [23]). Nevertheless, this approach is based on a discrete description of the boundary.

We have used an approach to represent the boundary with a continuous curve as an alternative to the gap approach. Our objective is thus to develop a viable methodology for solving the shape control problem directly through the control of a two-dimensional (2-D) planar contour without resorting to fixed (in the sense of the gap lines or the flux control points) discrete representations.

The Deformable Model Approach

The proposed boundary representation uses a geometric description that exploits the intrinsic nature of the plasma boundary as a constant flux (isoflux) 2-D curve on the poloidal cross section. Based on the fluid nature of the plasma, the magnetic flux configuration created by the plasma current and the external circuit currents can be regarded as the image of an object (that is, the plasma), and the plasma boundary as the object edge. The plasma boundary reconstruction can thus be viewed as a feature detection problem.

With reference to Figure 7, different ways of representing the shape reflect various original models that inspire the modeling process. For example, we can view the plasma as an open curve acting as a flexible rod bent by external forces and controlled with inner tension, a closed curve resembling the longitudinal section of a balloon held by the knot and corresponding to movements of inflation or deflation, or even as a twisted closed wire model.

From these preliminary considerations, the modeling involves decision processes that guide the automatic detection of shape boundaries. In particular, the nonlinearity introduced by the transition from limited to diverted configuration and vice-versa affects the choice of assumed shape topology.

Active Vision and Snakes

In the last few years, model-based vision has developed as a vigorously researched subject, which uses mathematical modeling to solve computational vision problems. In particular, deformable models have been used to guide the interpretation of camera-acquired images in noisy environments and to improve the robustness of object recognition [24], [25]. The fundamental idea of *deformable models* (or *templates*) is to accommodate a curve or surface into a data substratum based on 2-D or three-dimensional (3-D) image representations. A deformable model can deform according to the features of the object represented in the image, while preserving the characteristics of the model geometry. Geometry, physics, and approximation theory are combined, where geometry is responsible for the regularizing properties of the contour, physics gives the basis for a consistent representation, and approximation theory is used to fit the data.

On a more technical level, deformable models can be seen as elastic objects, which respond naturally to constraints and forces that are implicitly applied through an

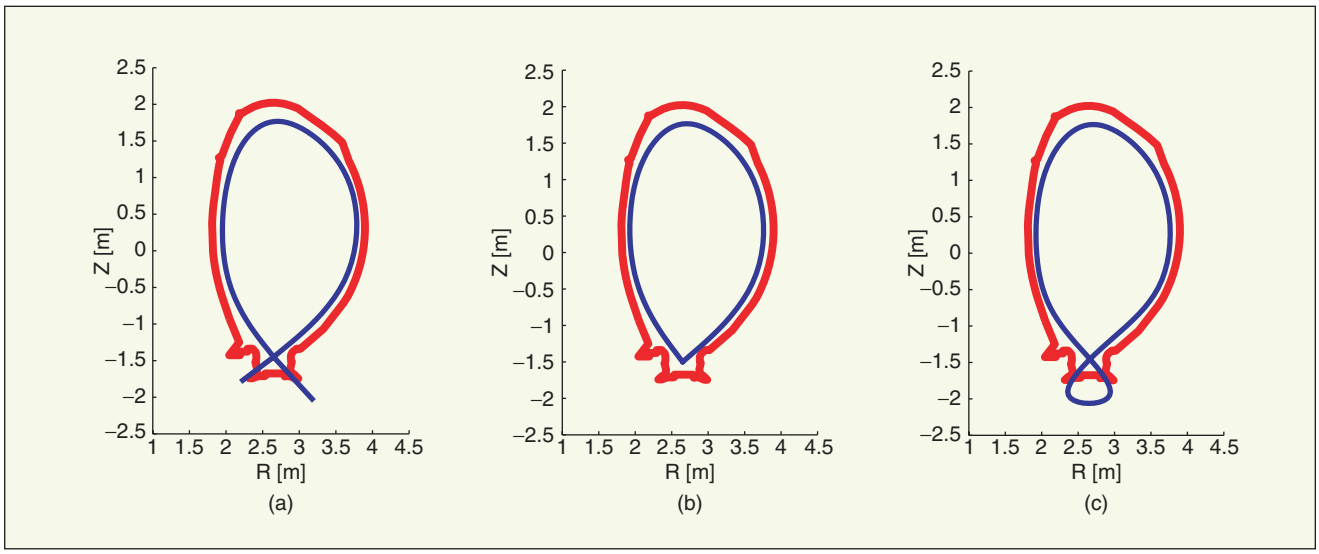

Figure 7. *Curve models for plasma boundary representation. Examples of deformable models are shown. (a) Flexible rod, (b) balloon, and (c) twisted closed wire. The active contour model and the geometry of the curve are chosen according to the reconstruction issues of interest.*

energy deformation function defined on the model itself. This energy function increases as the contour deforms from the natural rest shape, which represents the minimum energy state for the model. The deformation gives rise to elastic forces, which are treated as *internal forces* for the model. *Image forces* are also defined, which attract the contour to the features of interest.

In this framework, *snakes* [26] are parametric contour models that are obtained as energy-minimizing splines and that represent a special case of the multidimensional deformable

Tutorial 9: Plasma Heating and Current Drive

Several methods are used in experimental devices for heating and driving current in the plasma. Methods that have reached sufficient maturity for everyday experimental use include ohmic heating (OH) and current drive, neutral beam injection (NBI), and various forms of radio-frequency (RF) heating and current drive. Although these methods can accomplish both objectives, they are often configured with a primary purpose of either heating or current drive.

Ohmic current drive operates through a transformer action. Continuously changing current in one or more poloidal field coils produces a changing poloidal flux Ψ, known as the *ohmic flux*, at the plasma. The derivative of this flux defines an induced voltage $V = -d\Psi/dt$ known as the plasma *loop voltage*, which drives current in the plasma according to $LdI/dt + RI = V$, just as in a standard transformer. Here, the values L and R represent the plasma bulk equivalent self-inductance and resistance. Resistive losses in the plasma are responsible for the heating effect, hence the origin of the term *ohmic*.

RF heating is a process by which electromagnetic waves are transmitted into the plasma using antennas embedded in the interior plasma facing wall of the confinement vessel and a portion of their energy is absorbed by the plasma. Wave energy is coupled to the plasma particles primarily through resonant absorption. Resonant absorption occurs when the wave frequency is the same as a particle cyclotron frequency (see [1, Figure 8]), so that the wave's electric field increases the perpendicular velocity of the resonant particles. The direction of propagation of the RF waves determines whether this absorption results principally in heating the plasma or in a combination of heating and current drive. Wave propagation with a component parallel to the field lines can produce signficant current drive, while perpendicular acceleration principally produces heating. Typical ion cyclotron frequencies (ICH, ICCD) lie between 30 and 120 MHz, lower hybrid resonant frequencies (LHCD, for a plasma mode that is a hybrid of electron and ion cyclotron motions) lie between 1 and 8 GHz, and electron cyclotron resonant frequencies (ECH, ECCD) lie between 70 and 200 GHz. Current can also be driven by coupling to fast magnetosonic waves [fast wave current drive (FWCD)] or ion Bernstein waves (IBW) in the plasma [36].

NBI is the process by which neutral hydrogen or deuterium atoms are injected into the plasma at high speed and then become ionized through collisions with plasma particles. The resulting ions and electrons then become part of the plasma. The kinetic energy carried by the originally neutral atoms is transferred to the plasma by both the initial and subsequent collisions, resulting in an increase in thermal energy (temperature) of the plasma. Because the high-energy beam ions collide primarily with the plasma thermal electrons, NBI can produce significant current drive when the beam is injected tangentially (that is, in the toroidal direction). Tangentially injected neutrals also transfer their momentum to the plasma, thereby increasing the speed of rotation of the plasma fluid. Perpendicular injection of neutral beams produces only heating.

Another interaction between heating and current drive is produced by the resistivity of the plasma. In the same way that resistance relates current and voltage in a resistor, resistivity relates local current density (electrical current flow per square meter of plasma cross section) to local electric field in the plasma. The resistivity varies in both spatial distribution and in time (at a given location). The change in resistivity is primarily determined by the local temperature, with increasing temperatures responsible for decreasing resistivity. Thus, (local) heating of the plasma decreases the (local) resistivity, which in turn tends to increase the (local) current flow. Thus, while NBI drives significant noninductive current when injected tangentially, its primary effect is as a method of plasma heating, which has the collateral effect of broadening the current distribution and increasing the plasma current for the same loop voltage. In a similar manner, electron cyclotron heating (ECH), when used for heating the plasma, can also have the effect of increasing the local current in the (highly localized) deposition region.

model theory. In the classic formulation, the snake curve $\boldsymbol{C}$ is characterized by a function $\mathcal{E}(\boldsymbol{C})$, whose minimum value $\widetilde{\mathcal{E}}$ is given by the target contour shape $\widetilde{\boldsymbol{C}}$, that is,

$$\min_{\boldsymbol{C}} \mathcal{E}(\boldsymbol{C}) = \mathcal{E}\left(\widetilde{\boldsymbol{C}}\right) \equiv \widetilde{\mathcal{E}}.$$

The function $\mathcal{E}$, which is the energy of the contour $\boldsymbol{C}$ subject to the image, is constructed as the weighted sum of two contributions

$$\mathcal{E}(\boldsymbol{C}) = \underbrace{\int_0^1 \alpha(s)\left|\frac{\partial \boldsymbol{C}}{\partial s}\right|^2 + \beta(s)\left|\frac{\partial^2 \boldsymbol{C}}{\partial s^2}\right|^2 \mathrm{d}s}_{\mathcal{S}(\boldsymbol{C})} + \underbrace{\int_0^1 P(\boldsymbol{C}(s))\,\mathrm{d}s}_{\mathcal{P}(\boldsymbol{C})}, \tag{11}$$

where s is the curve parameter. The term $\mathcal{S}(\boldsymbol{C})$, which is the *internal energy* of the contour, measures the curve deformation, presenting a first-order derivative that characterizes the contour with tension and discourages stretching, and a second-order derivative that regulates the rigidity and counteracts the bending of the curve. Furthermore, these two contributions to $\mathcal{S}(\boldsymbol{C})$ are allowed to vary along the curve through the parameters α and β, which accounts for localized variations of the shape properties. In contrast, the energy term $\mathcal{P}(\boldsymbol{C})$, which couples the snake to the image, is computed by integrating a function P along the contour. The choice of P, which depends on the type of feature detection required in the specific application, is derived from the image intensity function directly or through the gradient. For example, if the user wants to determine the presence of light lines on a darker background, the appropriate intensity function is P; in a 256-gray-level representation, black lines and white lines correspond, respectively, to the largest and smallest values of P (255 and 0). If edges are the salient features, a more appropriate integrand function is the gradient of the image intensity, and the transition between different shades corresponds to peaks in the P function. Using the complete expression (11), the energy formulation accounts for the physics of the problem to be solved, through $\mathcal{P}(\boldsymbol{C})$, and the mathematics of the solution, through $\mathcal{S}(\boldsymbol{C})$.

Having defined the energy function, the solution procedure develops iteratively. After a contour is initialized and the energy value is computed, the curve is automatically deformed by minimizing $\mathcal{E}(\boldsymbol{C})$, guiding the location of the solution contour. After finding a satisfactory minimum $\widetilde{\mathcal{E}}$, the correspondent contour $\widetilde{\boldsymbol{C}}$ lies at the bottom of an energetic well, and the model tracks the motion of $\widetilde{\boldsymbol{C}}$ as the energy function evolves in time. Furthermore, a characteristic feature of the snake is that the model remains manageable because the degrees of freedom of the curve are not allowed to evolve independently, due to the geometrical constraints imposed through the internal energy term $\mathcal{S}(\boldsymbol{C})$. By exhibiting dynamic behavior, these deformable models are *active contours* [27].

The Plasma Picture and the Boundary Detection Problem

Beginning with the assertion that the information on the plasma boundary is embedded in the magnetic description of the configuration, it can be inferred that the flux map represents the object plasma. The 3-D map of the magnetic flux ψ in Figure 8(a) is based on information given by a magnetic reconstruction code such as XLOC. The processed output of the magnetic reconstruction (the flux map) defines the input for the generic boundary

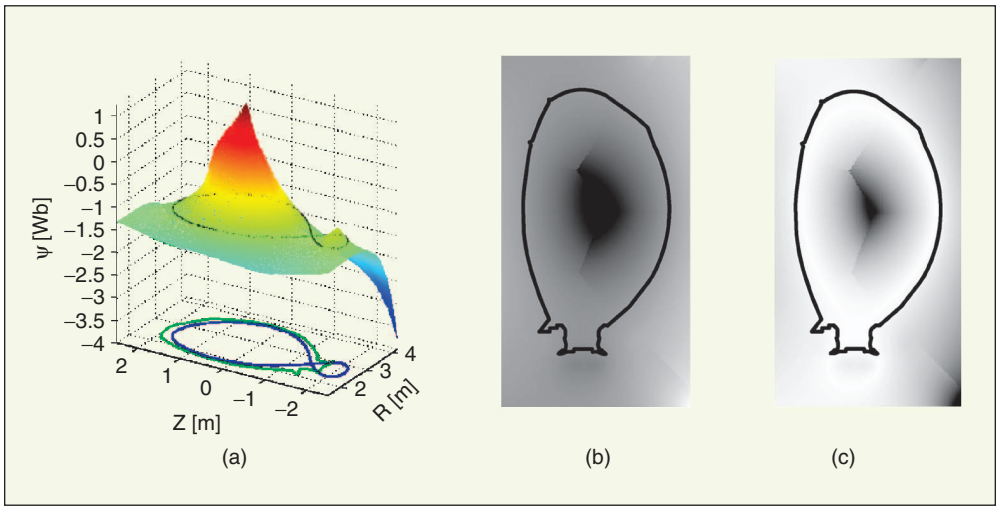

Figure 8. *The plasma image whose edge is to be detected. (a) The intensity of the flux map as defined by the XLOC algorithm is shown as a 3-D function to better appreciate the energy landscaping idea and the curve-sliding procedure. The first-wall and plasma boundary are superimposed to elucidate the meaning of the flux map. (b) The 2-D initial flux map is modified by subtracting the flux at (c) the boundary, defined as the maximum of the flux at the X point and over the plasma-facing surfaces. The resulting boundary image suggests the use of active vision techniques for edge detection.*

reconstruction tool. However, the intensity function is not yet suitable for automatic boundary detection and thus needs to be modified by using knowledge of the boundary flux value ψ_B to emphasize that the boundary is the edge of the object plasma and to enhance the detection capability [Figure 8(b)–(c)]. By exploiting the function

$$\widetilde{\psi}(r,z) = |\psi(r,z) - \psi_B|,$$

the boundary locus corresponds to the bottom of a potential well.

The tokamak, which is the most common machine for fusion research, is used to magnetically confine a gas in the plasma state inside a doughnut-shaped metallic chamber.

Active vision techniques for *feature detection* (that is, discerning parts or patterns in an image) are suitable for boundary reconstruction. The boundary is reduced to a 2-D dynamic contour that corresponds to the physical shape of the plasma in evolution, and the reconstruction problem can be reformulated as follows: Within the plasma region, find a regular curve that satisfies a specified constraint involving the flux map of the plasma cross section, and that depends on the flux value at the boundary. We emphasize that the shape of the boundary stems from the balance between the geometric elastic tension and the image-driven forces. With reference to the notation of the energy function in (11), the modified flux $\widetilde{\psi}$ plays the role of the image term P, while all nonmagnetic and often less-measurable effects are merged into geometric constraints and taken into account by an internal energy contribution.

Mimicking computer vision applications, boundary reconstruction can be achieved by allowing a snake curve χ to slide on a flux-based potential field so as to lock onto a local minimum. The contour χ corresponds to the curve $\boldsymbol{C}$ in the model (11) and to the plasma boundary location in physical terms. The initialization of the contour uses a curve corresponding to the border of the first wall (the boundary of the plasma region Ω_P in Figure 2). This position has a physical justification, in the sense that the first guess of the plasma location comprises the entire plasma region. The deformation of the curve, which is governed by a general shrinking movement implicit in the minimization of the integral function (11) proceeds with iterations based on a local algorithm that searches the neighborhood of the present contour solution for the curve with the minimum energy value. The size of the explored neighborhood, which defines the capture range of the snake, is predefined by the user, according to the coarseness of the flux map. Although there is no guarantee that this approach yields the optimal solution, experimental results have demonstrated stability, adequate speed of convergence, and accuracy in estimating the contour details. Thus, the algorithm reconstructs the location of the plasma boundary on the poloidal plane.

The snake model provides a simple plasma shape model, which requires limited preprocessing of the input flux map, due to the constraints imposed by the implementation of the algorithm for an eventual real-time use, with characteristic times of a few milliseconds.

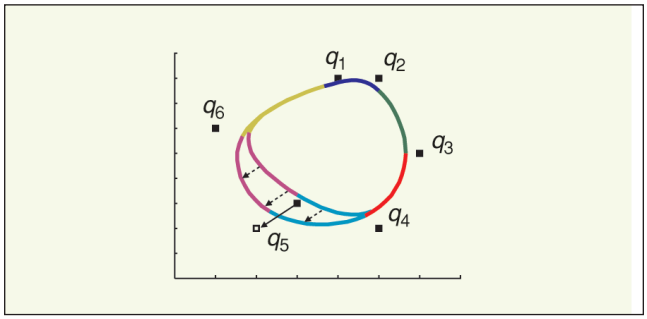

Figure 9. *The subcontours forming the B-spline. Individual subcontours of the spline, indicated using different colors, are each supervised by a different but overlapping subset of the full set of control points* $[q_1, q_2, \ldots, q_6]$. *Although the movement of one control point locally affects the shape of the curve, the deformation of the entire contour is fully described by the transformation from the full set of control points to the spline. As an illustration, the drawing shows the deformation of the shape due to the movement of the single control point* q_5, *affecting the location of the curve segments that list* q_5 *as one of the control points (segments in red, cyan, purple, and yellow).*

New Formulation of the Boundary

Several different candidate models for the plasma boundary are explored in [28]. A first deformable model, which evolves in the form of a closed curve [see Figure 7(b)], leads to the definition of an area metric (a metric based on area measurements) [29], [30]. Also, the built-in compactness of the representation guarantees limited deviation of the reconstructed contour from the actual boundary when moving into regions, such as in the X-point area, where the flux function is nearly flat. In this case, the local extrusion and deformation of part of the contour are limited by the energy minimization procedure, which tends to minimize

the curve length as well. Problems may arise when the plasma undergoes topological changes, for example, during the limited-to-diverted plasma transition. In this case, parameter tuning along with an automatic procedure for relaxing the smoothness constraints on the curve are needed to correct deformation of the boundary and create an X point. Since this deformation is regulated by the second-order derivative term in $\mathcal{S}$, it is reasonable to modify the β parameter. The desired behavior can be accomplished by means of either a global procedure, including a constant weight $\bar{\beta}$ in the flux difference

$$\beta(s) = |\psi(\chi(s)) - \psi_B|\,\bar{\beta}, \tag{12}$$

or by resorting to the function d measuring the Euclidean distance between the curve point $\chi(s)$ and the X-point location X

$$\beta(s) = d(\chi(s), X(r,z))\bar{\beta}, \tag{13}$$

if the coordinates of the X point are computed during the initial elaboration of the flux map and are provided to the reconstruction algorithm.

By adopting (12), the smoothness constraint is relaxed while the model curve χ that undergoes the deformation approaches the boundary curve since $\beta(s)$ tends to zero when the flux value computed on the curve points $\psi(\chi(s))$ tends to the boundary flux value ψ_B. A similar result can be obtained in the X-point area with (13). In this case, though, the effect is local since the parameter β goes to zero only at the X-point location, where the distance between $\chi(s)$ and X is zero.

The plasma boundary is the outermost closed flux surface entirely contained inside the vacuum vessel.

An alternative formulation of the energy-minimizing template based on a parametric B-spline representation of the contour [31] implicitly forces the smoothness of the curve, so that, to compute the deformation, calculation of only the image term $\mathcal{P}$ is required when updating the energy function [$\mathcal{E}(\boldsymbol{C}) = \mathcal{S}(\boldsymbol{C}) + \mathcal{P}(\boldsymbol{C})$ reduces to $\mathcal{E}(\boldsymbol{C}) = \mathcal{P}(\boldsymbol{C})$].

The B-spline is a piecewise polynomial curve, locally defined in simple form with low-order polynomial functions, yet at the same time globally smooth and flexible [32]. The global smoothness is enforced by requirements on matching derivatives at the points where the subcontours are connected. The interesting feature of the B-spline curve is that the shape of the contour can be modified by acting on a finite number of *control points* (Figure 9) that are related to points of the curve through a matrix transformation.

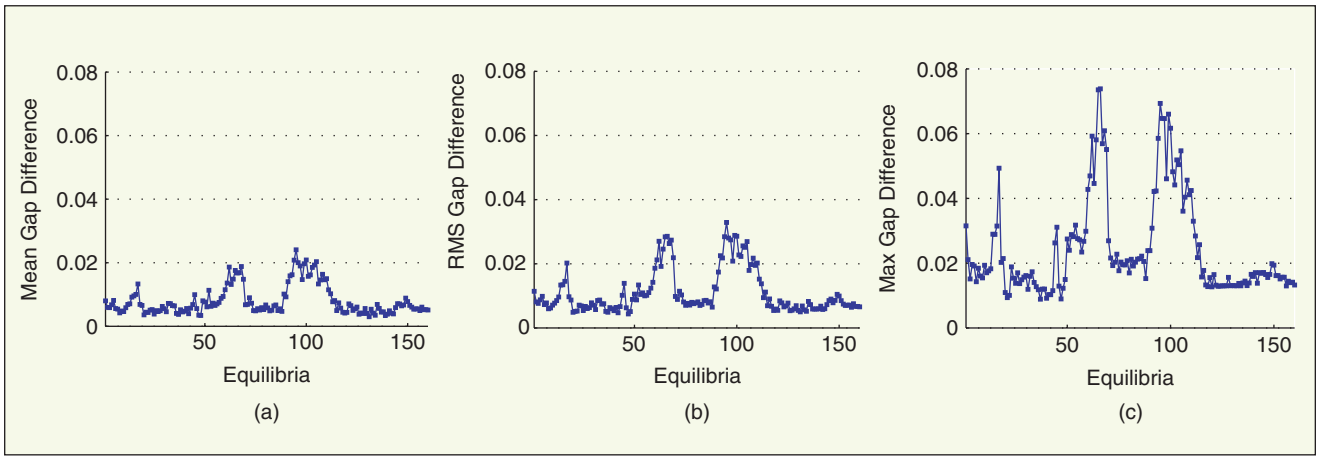

Figure 10. *Boundary reconstruction results at JET. These statistical plots show the difference between the boundary determined by the active contour reconstruction and the boundary defined by the gap values. Using equilibrium reconstruction codes, the magnitude error in using gaps to determine the boundary location has been estimated to be 2 and 4 cm, depending on the gap being measured [Figure 6(a)]. The difference between the active contour estimates and the gap-based estimates are approximately within this estimated error. (a) The mean values and (b) the root mean square (RMS) values, averaged along the contour, represent a displacement of the entire boundary, while (c) the maximum value indicates a local difference in the reconstructed shape, which typically occurs at the top part of the plasma. In this region the reconstruction of the boundary is less accurate because the plasma is more distant from the magnetic sensors and the flux function tends to flatten due to the presence of a top X point.*

While the plasma is evolving and the contour representing the boundary is deforming, the positions of the control points change due to the fact that the movement of the entire curve relies on the movement of the control points. In contrast, the matrices mapping the control points to the spline curve are time invariant since they are derived from the polynomial mathematical structure. Also, if the X-point position is available, placing a multiple control point at this location creates an angle along the contour. In doing so, the B-spline snake simulates the boundary behavior in proximity to the magnetic null, as obtained from the classic snake formulation by weighting the β parameter [as in (12) or (13)]. Thus, the spline approximation provides a linear mapping between the infinitely many points of the deformable contour and a limited set of control points in the (x, y)-plane.

Deformable models provide a new formulation of the plasma boundary as a continuous curve.

In the B-spline formulation of the snake, the plasma boundary curve χ is represented by the spline curve h, so that (11) reduces to

$$\mathcal{E}(\chi) = \int_0^1 P(h(s))\, \mathrm{d}s.$$

With this technique, energy minimization of the snake model is carried out over the points of the contour, which slides over the image surface. If the model is well behaved, the properties of the contour are captured by a limited set of control points, which provide compact representation and local control of the curve without diminishing the physical consistency of the solution.

Experience has shown that the snake model can locate the boundary and converge to a solution, while remaining sensitive to the tuning of the parameters in the energy expression. After verifying the correctness of the methodology, quantitative evaluations of the reconstruction accuracy are carried out using the JET database as a testbed. The values of the gap signals judging the correctness of the reconstruction, that is, the distances between the boundary defined by the set of gap

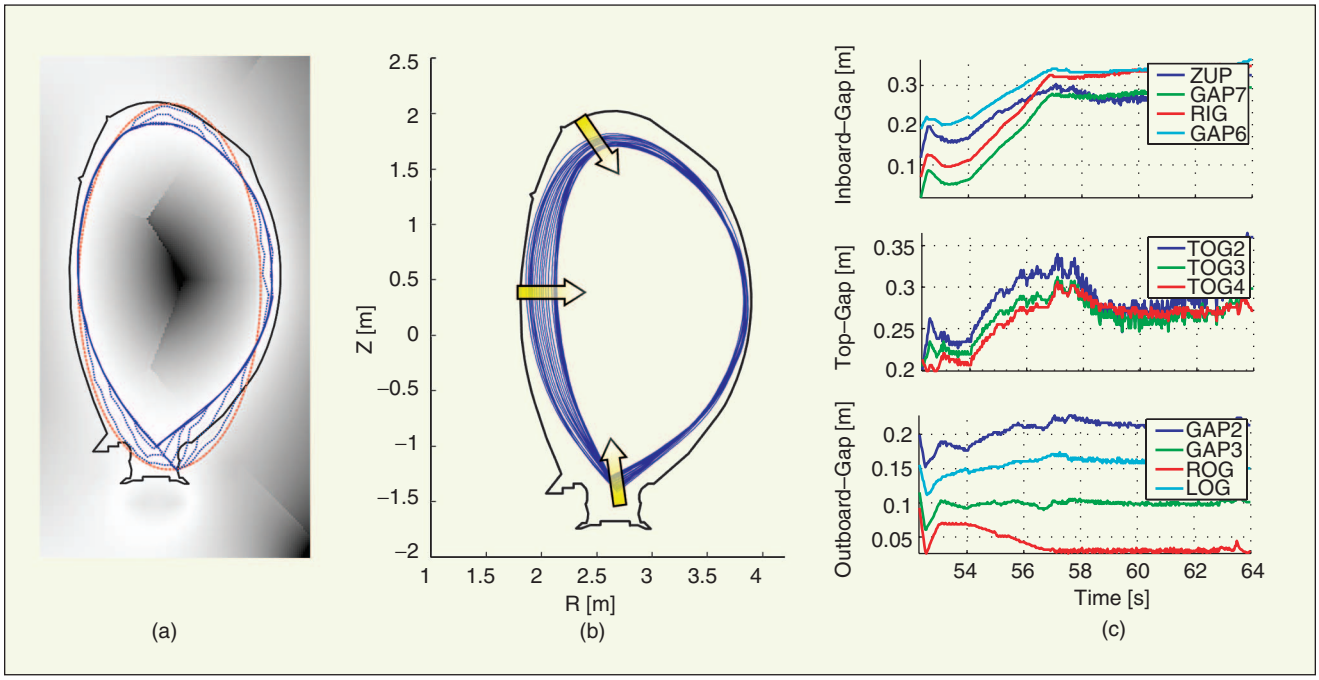

Figure 11. *Tracking a plasma shape with the active contour technique for JET pulse #57989. (a) Convergence to the initial shape. The dashed red line is the initial contour, the dotted curves are the iterations, and the blue solid line is the detected boundary. The curves shown for successive iterations follow the flux map grid points, and thus appear to be less smooth than the final contour. (b) The evolution during the discharge. The deformation of the plasma shape is evident. The configuration changes from a standard shape to a highly triangular one, with deformations mainly in the inner part of the boundary and the position of the X point. (c) The gap behavior is plotted as a function of time. The gaps, which are located as shown in Figure 6, are grouped according to the position on the poloidal cross section. From these waveforms the actual deformation of the shape is scarcely perceivable.*

values and the continuous curve, are evaluated. As can be seen in Figure 10, the accuracy required for the effective and safe execution of the experiment is achieved using the snake model, since the error is within the estimated error bar of the gap reconstruction. Moreover, although the accuracy of the reconstruction relies on the quality of the flux map, the snake model approach has an inherent robustness due to the geometric regularization, and thus artifacts due to errors in the magnetic information can be corrected.

The plasma boundary is determined by the magnetic field configuration. Thus, when the flux distribution changes in time, the plasma boundary changes shape. Since the plasma is assumed to evolve through equilibrium states, reconstruction of the movement is obtained *frame by frame* from single snapshots, namely, from flux maps produced at discrete time steps. Once the first boundary is detected, the shape can be tracked by using the previously computed contour. The capture range and number of iterations for convergence are significantly reduced after the first boundary reconstruction, improving the overall execution time of the algorithm. Since there is no time evolution model used in the active contour (as implemented thus far), reconstructing the plasma shape is a problem of *segmentation* (distinguishing a figure from the image background), more than tracking. The advantages are impressive when analyzing the evolution of the plasma shape during a pulse. As shown in Figure 11, the deformation is perceived more clearly than through examination of the evolution of gap signals.

New Formulation of the Plasma Parameters

Describing the boundary as a curve on the poloidal plane introduces a new calculation, if not a new definition, of the global plasma quantities κ and δ. Elongation and triangularity can now be computed using the continuous boundary locus instead of resorting to point-based local information as in (8)–(10).

The plasma boundary reconstruction can be viewed as a feature detection problem.

The definition (7) of the elongation κ based on the area of the cross section serves as an illustrative example, where A and a can now be directly and accurately computed. Similarly, upper and lower triangularity can be given as the area ratios

$$\delta_{\mathrm{UP}} = \frac{A_{\mathrm{UPout}} - A_{\mathrm{UPin}}}{A_{\mathrm{UPout}} + A_{\mathrm{UPin}}},$$
$$\delta_{\mathrm{LOW}} = \frac{A_{\mathrm{LOWout}} - A_{\mathrm{LOWin}}}{A_{\mathrm{LOWout}} + A_{\mathrm{LOWin}}},$$

where the area sector definitions are deduced from Figure 4. With this approach, the triangularity parameters account for the effective curvature of the plasma boundary and represent a more refined description of the plasma boundary shape than the analogous quantities obtained from point information.

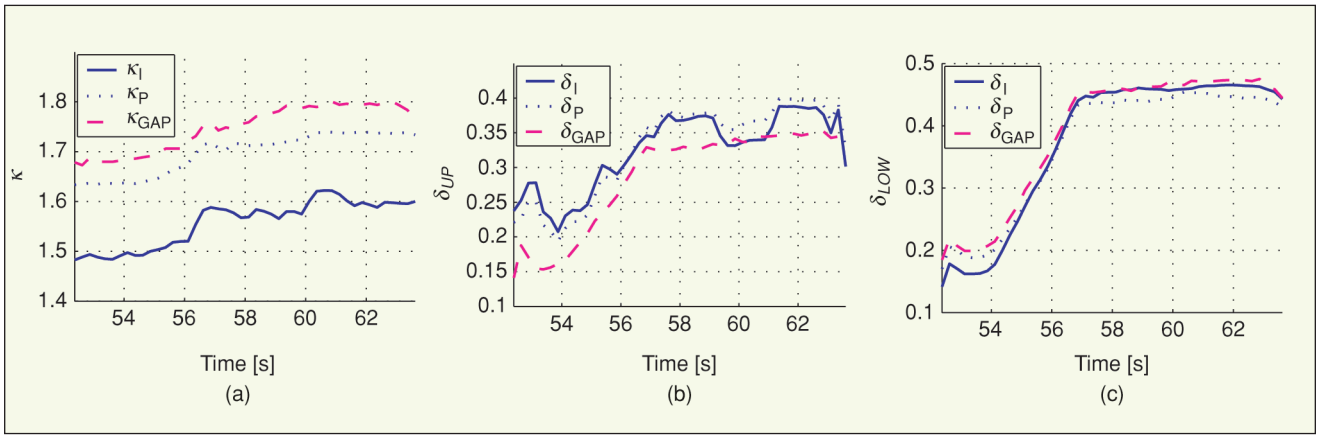

Figure 12. *Tracking the global parameters for JET pulse #57989, where subscripts* I, P, *and* GAP *indicate that the parameter is calculated using the integral snake representation, the pointwise information, and the gap values, respectively. (a) The elongation κ. The (b) upper and (c) lower triangularity δ_{UP} and δ_{LOW}. Although all of the quantities exhibit similar behavior during the discharge, the parameters obtained from the snake representation provide a more detailed description of the shape deformations than those computed based on gap distances.*

This boundary description is applied to JET plasmas, using the active contour reconstruction to provide the boundary curve for the area calculations, while the computed parameters are compared with the corresponding quantities obtained from point information. For the plasma evolution of a highly shaped pulse, the shape deformation shown in Figure 11 is reflected in the parameter behaviors of Figure 12. Elongation and triangularity measurements yield interesting considerations. For example, the different definitions for elongation κ—one computed from gap values, the other from area quantities—cause the computed results to take on different ranges of values. Moreover, elongation and triangularity computed according to the contour boundary description exhibit dynamic behavior that is more nervous than the respective gap-based values (8)–(10), since these parameters are not explicitly regulated by gap control. Although all of the parameter representations show similar behavior, the form derived from the continuous description is more realistic since the calculation accounts for the curvature of the contour.

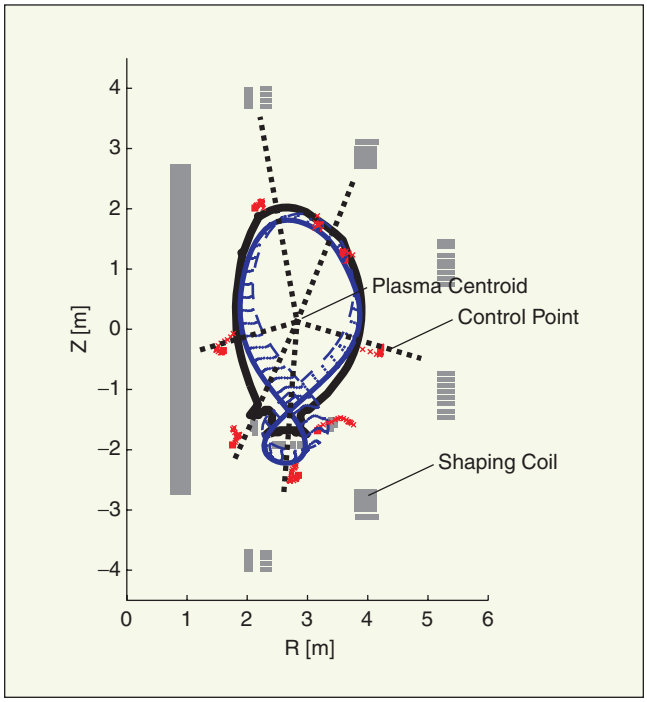

Figure 13. *B-spline control point movements during convergence of the boundary detection algorithm. This figure suggests a correlation between the location of the control points that parameterize the spline model of the boundary and the position of the shaping coils, since some of the control points are moving along a line connecting the active coil to the plasma centroid (black dotted lines). By producing a map between the external actuators and the spline control points, it is possible to control the plasma boundary by taking into account the entire curve. The control points are indicated with red crosses during the iteration (corresponding to the blue dotted curves) and with square dots when the boundary is detected (blue solid contour). The coil sections are visible in gray blocks.*

Application to Shape Control

Reconstruction using splines facilitates control action based on the set of control points over a 2-D space but facilitates control of the entire contour on the poloidal section. To produce a useful description of the contour, the number of control points is kept constant and close to the number of independent actuators. The structure of the spline curve is chosen such that the location of each control point is correlated with active circuit effectiveness to deform or regulate the plasma shape as well as with the position of the coils on the tokamak cross section. We can postulate that a transformation exists from the space of actuator currents to the space of control points, which corresponds to the transformation between the magnetic configurations attainable in a specific tokamak and the resulting plasma shapes. In producing a mapping between actuator currents and spline control points, a controller can be designed that acts on the external active circuits to achieve the desired plasma shape.

As an illustration, Figure 13 shows the movements of the control points during the convergence of the boundary detection algorithm. Ambiguous cases may arise, however, particularly in devices like JET, where the shaping circuits are comprised of series-connected multiple toroidal windings of copper conductor whose coordinates in the (r, z)-plane are distributed spatially [1, Figure 5]. Therefore, because of the different positions in the poloidal plane, the control actions cannot be assigned with confidence to one coil instead of another. Nevertheless, it is possible to distinguish some influence in the divertor region where the coils are controlled separately and on the midplane due to the action of the radial field.

For this reason, further studies were conducted on the ITER-FEAT machine design, where the action of each shaping coil is commanded separately, enabling better assessment and understanding of the relationships among curve shape, control points, and the action of actuators. These analyses required extensive use of the MAXFEA equilibrium evolution code. It appears clear that the number of spline control points dictated by control requirements (number of control points equal to number of available independent actuators) yields only a rough approximation of the boundary shape. We have thus implemented a more precise definition of the boundary spline curve using a larger number of control points to measure the distance of the boundary from a shape target model. The initial 2-D spline curve representing the boundary is thus reduced to a one-dimensional spline representing the distance function, providing a smaller set of control point parameters that summarize the geometric configuration of the plasma cross section. It is thus possible to design a spline control

scheme whose performance is comparable to that of a classic gap controller. The results of control simulation are encouraging, showing that convergence to zero of the control point position error, obtained by using the spline controller, implies the regulation of the gap values as well. A complementary behavior is not ensured by the gap control technique, which is not similarly efficient at controlling the spline curve [33].

Furthermore, preliminary work using the spline controller, and based on the area definition of both triangularity and elongation, confirms that global properties can be better recovered from a shape disturbance using the contour approach than by the gap controller, although some effort is still necessary to provide reliable measurements of the controlled variables. Nevertheless, the idea is appealing since many high-performance scenarios require control of global parameters.

An interesting application is the problem of optimal coupling of the heating antennas with the plasma (see "Tutorial 9"). In this case, the plasma boundary must be maintained at a fixed distance from the wall over the entire spatial extent of the antennas, a requirement that is more easily posed using the contour approach than when controlling a discrete number of boundary points. The regularity of the boundary curvature of specific sections of the plasma surface simplifies the description of the deformation in front of the devices into principal movements (tilting and displacement orthogonal to the antenna).

Discussion and Conclusions

In this article, we presented the problem of plasma boundary reconstruction in relation to shape control and discussed different approaches sharing the same objective of guaranteeing accuracy and robustness of plasma boundary control. We stressed that shape measurement is a delicate operation because it is based on calculations.

Deformable models provide a new formulation of the plasma boundary as a continuous contour, which facilitates more accurate estimation of global shape parameters, able to describe the plasma evolution in a realistic way. Moreover, the representation of the plasma boundary as a curve is immune from the problematic issues due to the use of local information and results in less sensitivity to noise. The methodology provides an intuitive and elegant tool for plasma boundary representation and dynamic reconstruction, appealing for plasma shape diagnostics and control, since the technique enhances the control accuracy of both the shape global parameters and the boundary itself. At the same time, this description shows new control variables with respect to gaps or flux errors, when we consider the spline control points, or different value ranges, when the global quantities are defined according to area ratios. The active contour representation can be used either in the gap control methodology or to control global quantities. For example, the definition of gap clearance can be modified by computing the minimum distance from the boundary to the first wall. Still, it is more difficult to control the minimum distance along a contour than the minimum distance over a set of gaps.

The results of the analyses performed on JET and on ITER support the validity of the snake reconstruction methodology, consistent with the gap controller boundary information, since the response of the active contour approach is tested against the information available in real time to the system (employed in the case of JET, designed in the case of ITER). The flux maps used for reconstruction are obtained either from a reconstruction code operating on real experimental data or from an MHD equilibrium code. The next step in evaluating the new approach consists of more exhaustive and fully real-time tests on existing machines. At the same time, work is in progress on magnetic diagnostics [34] and flux reconstruction modeling [35] to further develop capabilities for shape reconstruction.

Acknowledgments

We are grateful to Consorzio RFX—Associazione EURATOM-ENEA per la Fusione for the support provided for our work. We are also pleased to acknowledge Dr. Mario Cavinato for his precious help with the MAXFEA code and Simone Simionato and Anton Soppelsa for their enthusiasm and skill. Finally, special thanks to our colleagues for many valuable discussions on this topic and for their kind and precise review of the manuscript, in particular Dr. Mike Walker at General Atomics—DIII-D and Dr. Phil Morgan at JET—EURATOM-UKAEA Fusion Association.

References

[1] A. Pironti and M.L. Walker, "Fusion, tokamaks, and plasma control," *IEEE Control Syst. Mag.,* vol. 25*,* no. 5, pp. 30–43, 2005.

[2] G. Ambrosino and R. Albanese, "Magnetic control of plasma, current, position, and shape in tokamaks," *IEEE Control Syst. Mag.*, vol. 25, no.5, pp. 76–92, 2005.

[3] J. Wesson, *Tokamaks*. Oxford, UK: Clarendon Press, 1997.

[4] J.P. Freidberg, *Ideal Magnetohydrodynamics*. New York: Plenum, 1987.

[5] R. Albanese, J. Blum, and O. DeBarbieri, "Numerical studies of the next European torus via the PROTEUS code," in *Proc. 12th Conf. Numerical Simulation Plasmas*, San Francisco, CA, 1987, IT4.

[6] M. Cavinato, A. Kavin, V.E. Lukash, and R.R. Khayrutdinov, "Non-linear simulations by numerical magneto hydro dynamics equilibrium codes in ITER-FEAT," in *Proc. IEEE Int. Conf. Control Applications (CCA),* Anchorage, AK, 2000, pp. 406–411.

[7] D.W. Swain and G.H. Neilson, "An efficient technique for magnetic analysis of noncircular, high-beta tokamak equilibria," *Nucl. Fusion*, vol. 22, no. 8, pp. 1015–1030, 1982.

[8] F. Hofmann and G. Tonetti, "Fast identification of plasma boundary and X-points in elongated tokamaks," *Nucl. Fusion*, vol. 28, no. 3, pp. 519–522, 1988.

[9] F. Alladio and F. Crisanti, "Analysis of MHD equilibria by toroidal multipolar expansions," *Nucl. Fusion*, vol. 26, no. 9, pp. 1143–1164, 1986.

[10] L.L. Lao, H. St. John, R.D. Stambaugh, A.G. Kellman, and W. Pfeiffer, "Reconstruction of current profile parameters and plasma shapes in tokamaks," *Nucl. Fusion*, vol. 25, no. 11, pp. 1611–1622, 1985.

[11] F. Sartori, A. Cenedese, and F. Milani, "JET real-time object-oriented code for plasma boundary reconstruction," *Fusion Eng. Des.*, vol. 66–68, pp. 735–739, 2003.

[12] E.W. Weisstein, (1999). Green's Function. *MathWorld—A Wolfram Web Resource* [Online]. Available: http://mathworld.wolfram.com/GreensFunction.html

[13] J.R. Ferron, M.L. Walker, L.L. Lao, H.E. St. John, D.A. Humphreys, and J.A. Leuer, "Real-time equilibrium reconstruction for tokamak discharge control," *Nucl. Fusion*, vol. 38, no. 7, pp. 1055–1066, 1998.

[14] L.E. Zacharov and V.D. Shafranov, "Equilibrium of a toroidal plasma with noncircular cross section," *Sov. Phys. Tech. Phys.*, vol. 18, no. 2, pp. 151–156, 1973.

[15] F. Hofmann and S.C. Jardin, "Plasma shape and position control in highly elongated tokamaks," *Nucl. Fusion*, vol. 30, no. 10, pp. 2013–2022, 1990.

[16] S. Puppin M.E. Angoletta, D.J. Campbell, J.J. Ellis, M. Garribba, M. Lennholm, F. Milani, D. O'Brien, F. Sartori, and R. Sartori, "Real-time control of plasma boundary in JET," in *Proc. 19th Symp. Fusion Tech. (SOFT)*, Lisbon, Portugal, 1996, pp. 949–953.

[17] A. Cenedese and F. Sartori, "Plasma position and current control management at JET," in *Proc. 42nd Conf. Decision Control (CDC)*, Maui, Hawaii, 2003, pp. 4628–4633.

[18] Y. Shimomura, R. Aymar, V. Chuyanov, M. Huguet, R. Parker, and ITER Joint Central Team, "ITER overview," *Nucl. Fusion*, vol. 39, no. 9Y, pp. 1295–1308, 1999.

[19] A. Portone, "Design of the ITER-FEAT plasma control system by a frequency separation approach," *Fusion Eng. Des.*, vol. 56–57, pp. 789–794, 2001.

[20] A. Pironti and A. Portone, "Optimal choice of the geometrical descriptors for tokamak plasma shape control," *Fusion Eng. Des.*, vol. 43, no. 2, pp. 115–127, 1998.

[21] A. Beghi, "An application of selective modal analysis to tokamak modeling and control," *IEEE Trans. Contr. Syst. Technol.*, vol. 9, no. 4, pp. 574–589, 2001.

[22] G. Ambrosino, M. Ariola, A. Pironti, and F. Sartori, "A new shape controller for extremely shaped plasmas in JET," *Fusion Eng. Des.*, vol. 66–68, pp. 797–802, 2003.

[23] M. Ariola and A. Pironti, "Plasma shape control for the JET tokamak," *IEEE Control Syst. Mag.*, vol. 25, no.5, pp. 65–75, 2005.

[24] L.H. Staib and J.S. Duncan, "Boundary finding with parametrically deformable models," *IEEE Trans. Pattern Anal. Machine Intell.*, vol. 14, no. 11, pp. 1061–1075, 1992.

[25] N. Ayache, "Medical computer vision, virtual reality and robotics," *Image Vis. Comput.*, vol. 13, no. 4, pp. 295–313, 1995.

[26] A. Kass, A. Witkin, and D. Terzopoulos, "Snakes: Active contours models," *Int. J. Comput. Vis.*, vol. 1, no. 4, pp. 321–331, 1987.

[27] A. Blake and M. Isard, *Active Contours*. London, UK: Springer, 1998.

[28] A. Cenedese, A. Beghi, D. Ciscato, and F. Sartori, "Active contour approach for plasma boundary reconstruction," *Fusion Eng. Des.*, vol. 66–68, pp. 675–680, 2003.

[29] J.M. Berg and K. Holmström, "On parameter estimation using level sets," *SIAM J. Control Optim.*, vol. 37, no. 5, pp. 1372–1393, 1999.

[30] V.V. Kindratenko, "On using functions to describe the shape," *J. Math. Imaging Vis.*, vol. 18, no. 3, pp. 225–245, 2003.

[31] P. Brigger, J. Hoeg, and M. Unser, "B-spline snakes: A flexible tool for parametric contour detection," *IEEE Trans. Image Processing*, vol. 9, no. 9, pp. 1484–1496, 2000.

[32] E.W. Weisstein, (1999). B-Spline. *MathWorld—A Wolfram Web Resource* [Online]. Available: http://mathworld.wolfram.com/B-Spline.html

[33] A. Beghi, M. Cavinato, A. Cenedese, D. Ciscato, S. Simionato, and A. Soppelsa, "An integral approach to plasma shape control," *Fusion Eng. Des.*, to be published 2005.

[34] A. Cenedese, R. Albanese, G. Artaserse, M. Mattei, F. Sartori, and JET-EFDA Contributors, "Reconstruction capability of JET magnetic sensors," *Fusion Eng. Des.*, to be published 2005.

[35] A. Cenedese, F. Sartori, and M. Macuglia, "Development of a fixed-position filamentary plasma model based on the current moment description," *IEEE Proc. Sci, Meas. Tech.*, vol. 151, no. 6, pp. 484–487, 2004.

[36] M. Porkolab, "Review of RF heating," in *Proc. Int. School Plasma Physics*, Varenna, 1977, p. 339.

Alessandro Beghi received the laurea degree (cum laude) in electrical engineering in 1989 and the Ph.D. degree in control system engineering in 1993 from the University of Padova, Italy. In 1992, he was a visiting scholar at the Department of Electrical and Computer Engineering and the Institute of Theoretical Dynamics of the University of California at Davis. From 1993 to 1994 he was with the LADSEB-CNR, Padova, Italy, on a postdoctoral fellowship. In 1994, he joined the Dipartimento di Ingegneria dell'Informazione (DEI), University of Padova, Italy, where he is currently an associate professor. He is also affiliated with the Centro Ricerche Fusione (Center for Research on Fusion) of the University of Padova, Italy. Since 1996, he has been collaborating at the International Thermonuclear Experimental Reactor (ITER) experiment as a member of the European Home Team. His research interests include stochastic modeling and control, filtering and identification, and model reduction.

Angelo Cenedese (angelo.cenedese@dei.unipd.it) received the laurea degree in electronic engineering in 1999 from the University of Padova, Italy, and in 2000, he completed a postgraduate course on plasma physics and thermonuclear device engineering with the Electrical Engineering Department and Consorzio RFX—EURATOM Fusion Association, Padova, Italy. From 2002 to 2004, he was a visiting student at JET Laboratories in Culham, UK. Since receiving his Ph.D. from the University of Padova in 2004, he has been responsible for software tasks for the EFDA-JET Enhancement on Magnetic Diagnostics. In 2004, he joined the Dipartimento di Ingegneria dell'Informazione (DEI), University of Padova, Italy, on a postdoctoral fellowship. His research interests are in the fields of identification, modeling and control, and active vision. He can be contacted at D.E.I. and Centro Ricerche Fusione, Università di Padova, Via Gradenigo 6/B, I-35131 Padova, Italy.